

Role of electron scattering on the high-order harmonic generation from solids

Chang-Ming Wang,¹ Nicolas Tancogne-Dejean,¹ Massimo Altarelli,¹ Angel Rubio,^{1,*} and Shunsuke A. Sato^{2,1,†}

¹*Max Planck Institute for the Structure and Dynamics of Matter,
Luruper Chaussee 149, 22761 Hamburg, Germany*

²*Center for Computational Sciences, University of Tsukuba, Tsukuba, Ibaraki 305-8577, Japan*

(Dated: January 12, 2022)

We extend the semi-classical trajectory description for the high-order harmonic generation (HHG) from solids by integrating the effect of electron-scattering. Comparing the extended semi-classical trajectory model with a one-dimensional quantum mechanical simulation, we find that the multi-plateau feature of the HHG spectrum is formed by Umklapp scattering under the electron-hole acceleration dynamics by laser fields. Furthermore, by tracing the scattered trajectories in real-space, the model fairly describes the emitted photon energy and the emission timing of the HHG even in the higher plateau regions. We further consider the loss of trajectories by scattering processes with a mean-free-path approximation and evaluate the HHG cutoff energy as a function of laser wavelength. As a result, we find that the trajectory loss by scattering causes the wavelength independence of the HHG from solids.

I. INTRODUCTION

Light-matter interactions have been an important subject in physics from both fundamental and technological points of view [1–4]. Intense light may couple with matter nonlinearly and can induce nonlinear optical effects [5–9], such as the second order harmonic generation [10]. Once field strength of light becomes extremely large, non-perturbative and highly-nonlinear phenomena may be induced. A primary example of such phenomena is the high-order harmonic generation (HHG) [11–13], which is an extreme photon-upconversion process via strongly-nonlinear light-matter interactions. This process has been observed from atomic gases decades ago [14, 15], and the gas-phase HHG further opened a novel technology to generate ultrashort laser pulses with attosecond duration, offering a novel avenue to explore ultrafast real-time electron dynamics in matter [16–21]. Recently, the HHG from solid-state materials has been systematically observed [22]. It has been demonstrated that the solid-state HHG shows distinct fundamental features from the gas-phase HHG, such as the linear scaling of the cutoff energy with respect to the field strength [22–24], the wavelength independence of the cutoff energy [22, 24, 25], and the enhancement of HHG by elliptically-polarized light [26, 27]. It has also been shown that the competition of mechanisms between atomic-like and solid-like responses in two-dimensional systems further enriches the HHG spectra [28–30]. These distinct features of the solid-state HHG have been drawing great attention because it offers a novel possibility to investigate ultrafast electron dynamics in matter and may open a path to novel light sources [31].

The mechanism of the HHG from gases has been understood by the semi-classical trajectory model; so-called

three-step model [32–34]. The model consists of the following three steps: (i) An electron is ionized from an atom or molecule due to a strong laser field. (ii) The ionized electron is accelerated by the laser field in vacuum. (iii) The accelerated high-energy electron returns to the parent ion due to the oscillatory field and recombines, emitting high energy photons. The three-step model describes well the features of the gas-phase HHG such as the cutoff energy. The semi-classical trajectory model has been further extended to the solid-state HHG [35], integrating the electronic band dispersion of solids as the crystal-momentum-dependent effective mass of electron-hole pairs. In this regard, the extended semi-classical trajectory model still treats the dynamics of electron-hole pairs as that of free particles. However, in contrast to ionized electrons in vacuum, electrons in solids may be easily scattered by ions, other electrons, defects and so on. Therefore, electron scattering is expected to play an important role for the HHG from solids.

Despite the great effort to study the mechanism of the HHG from solids, the role of the electron scattering has not been investigated yet in the context of the semi-classical trajectory description. In this paper we consider an extension of the real-space semi-classical trajectory model by incorporating scattering effects in solids. The generalization is carried out by branching a classical trajectory into multiple trajectories whenever a scattering event occurs. We compare the scattering-integrated semi-classical trajectory model with one-dimensional quantum dynamical simulations, and explore a role of Umklapp scattering in the HHG from solids. Furthermore, we extend our modeling with the mean-free-path approximation and elucidate the effect of the scattering to the wavelength scaling of the HHG cutoff.

This paper is organized as follows: In Sec. II we first revisit the semi-classical trajectory model for HHG from solids. Then, we extend the model by incorporating the scattering effect. In Sec. III we examine the role of the scattering in the HHG with the model, comparing with

* angel.rubio@mpsd.mpg.de

† ssato@ccs.tsukuba.ac.jp

the one-dimensional quantum model. Finally our findings are summarized in Sec. IV. In this work, atomic units are used unless stated otherwise.

II. METHODS

A. Semi-classical trajectory model for solid-state HHG

Here, we first revisit a semi-classical trajectory model for the solid-state HHG [35] to further introduce the scattering effect into it. The semi-classical trajectory model, or the so-called *three-step model*, has been originally proposed to describe the HHG from noble gases [32–34]. The model properly describes key features of the HHG spectrum such as the cutoff energy. Recently, the semi-classical trajectory model was extended to the solid-state HHG [35]. In the solid-state semi-classical trajectory model, the HHG is described by the following three steps:

1. Creation of an electron-hole pair by exciting an electron from a valence band to a conduction band at the optical gap of the solid.
2. Acceleration of the electron-hole pair by an external laser field.
3. Emission of a high-energy photon by the recombination of the accelerated electron-hole pair.

The major difference of the solid-state semi-classical trajectory model from the corresponding gas-phase model is the treatment of the acceleration of particles in the second step: since ionized electrons travel in vacuum in the gas-phase model, they can be treated as free charged-particles, which have a parabolic energy dispersion, $\epsilon(\mathbf{k}) = \hbar^2 \mathbf{k}^2 / 2m_e$ with the wavenumber \mathbf{k} . In contrast, the dynamics of electron-hole pairs in solids is not generally described by the simple parabolic energy dispersion but requires more complex anharmonic dispersion reflecting the solid-state electronic band structure. Thus, the solid-state semi-classical trajectory model can be seen as a generalization of the gas-phase model by changing the electron mass m_e to the effective electron-hole mass,

$$\mu_{ij} = \left[\frac{\partial^2}{\partial k_i \partial k_j} (\epsilon_{c\mathbf{k}} - \epsilon_{v\mathbf{k}}) \right]^{-1}, \quad (1)$$

where $\epsilon_{b\mathbf{k}}$ is the band dispersion of valence ($b = v$) and conduction ($b = c$) bands.

Based on the semi-classical trajectory model, the relative position $\mathbf{x}(t)$ of an electron-hole pair created at the time t_0 can be described as [35]:

$$\mathbf{x}(t) = \int_{t_0}^t dt' \mathbf{v}(\mathbf{K}(t')), \quad (2)$$

where $\mathbf{K}(t) = \mathbf{k} + \mathbf{A}(t)$ is the shifted wavevector due to the applied vector potential $\mathbf{A}(t)$ by the acceleration theorem. The relative electron-hole velocity $\mathbf{v}(\mathbf{k})$ is determined by the electron-hole energy dispersion as

$$\mathbf{v}(\mathbf{k}) = \mathbf{v}_c(\mathbf{k}) - \mathbf{v}_v(\mathbf{k}) = \frac{\partial}{\partial \mathbf{k}} [\epsilon_{c\mathbf{k}} - \epsilon_{v\mathbf{k}}]. \quad (3)$$

In the semi-classical trajectory model, an electron-hole pair is assumed to be created at the band gap with zero distance $\mathbf{x}(t_0) = 0$. Then, the trajectory $\mathbf{x}(t)$ is evolved with Eq. (2). In the final step, the electron-hole pair is recombined at time t_r and emits a photon when the electron and hole come back to the same position $\mathbf{x}(t_r) = 0$. The emitted photon energy corresponds to the energy of the recombined electron-hole pair, $\epsilon_{c\mathbf{K}(t_r)} - \epsilon_{v\mathbf{K}(t_r)}$.

B. Electron scattering effect in the semi-classical trajectory model

In the above semi-classical model, dynamics of ionized electrons or created electron-hole pairs is treated as independent free particles. This treatment is accurate enough to describe the HHG from dilute gases. However, in solids, electrons and holes can be scattered by phonons, other electrons and holes, impurities and many other processes. Therefore, the free-particle treatment without scattering processes is not complete to describe the solid-state HHG. The importance of such scattering processes could also be seen in the recently observed multi-plateau feature in HHG spectra. Unlike many HHG spectra from semiconductors featuring single plateau, the experiments using noble-gas solids [36] demonstrate the multiple plateaus feature in the HHG spectra. Furthermore, it has been demonstrated that such multi-plateau feature can be theoretically described by ladder-climbing process [37], which is conceptually based on Umklapp scattering. Thus, the multi-plateau feature could be seen as the consequence of the scattering effect. However, in the previous study proposing the ladder-climbing process, only the k -space (crystal momentum space) semi-classical trajectories have been considered, and it was assumed that electron-hole pairs can recombine at any instance of time. As a result, an electron and a hole are allowed to recombine and emit a photon no matter how far they are separated in real space. In this work, we integrate Umklapp scattering effect into the semi-classical trajectory model using both real- and k -space trajectories. This allows us to obtain the information of recombination time for electron-hole pairs and thereby refine the solid-state semi-classical trajectory model.

The incorporation of Umklapp scattering effect with the semi-classical trajectory model is carried out as follows:

1. Creating an electron-hole pair at the time t_0 by exciting an electron from a valence band to a conduction band at the Bloch wavevector, \mathbf{k}_0 that corresponds to the optical gap of the solid.

2. Propagating the trajectory in real-space, $\mathbf{x}(t)$ with Eq. (2) and the trajectory in k -space, $\mathbf{k}_0 + \mathbf{A}(t) - \mathbf{A}(t_0)$, with the acceleration theorem.
3. Branching a trajectory into scattered and non-scattered trajectories when the trajectory reaches the Brillouin zone edge. Here, Umklapp scattering is described as the sudden shift of the accelerated Bloch vector $\mathbf{K}(t) \rightarrow \mathbf{K}(t) \pm n\mathbf{b}$ with the reciprocal lattice vector, \mathbf{b} and an integer n . The details of the scattering is depicted in Fig. 1. After the scattering, the branched trajectories are propagated in the same way described in the step 2.
4. Recombining the electron-hole pair at time t_r when $\mathbf{x}(t_r) = 0$, and emitting a photon whose energy corresponds to the energy difference of the electron-hole pair, $\epsilon_{c,\mathbf{K}(t_r)} - \epsilon_{v,\mathbf{K}(t_r)}$.

Figure 1 shows a schematic picture of the branching procedure discussed above. The red-solid line shows an unfolded conduction band while the blue-solid line shows a valence band. The replicated conduction bands shifted with the reciprocal lattice vector are described as the red-dashed lines. In Fig. 1, the arrow, ①, describes the excitation of an electron from the top of the valence band to the bottom of the conduction band. The arrow, ②, indicates the acceleration of the electron from the conduction bottom to the Brillouin zone edge. At the Brillouin zone edge, the conduction bands have a crossing, or they may have an avoid-crossing. After the crossing at the Brillouin zone edge, the electron trajectory may diabatically follow the red-solid line as depicted with the arrow, ③, or may be switched to the red-dashed line as ④. Since the red-dashed lines are nothing but the replicated bands with the crystal momentum shift by the reciprocal lattice vector, the switching of the bands is nothing but Umklapp scattering at the Brillouin zone edge. In general, where bands are crossing, the inter-band transition may occur due to scattering processes. In this work, such scattering effect is incorporated with switching of the trajectory on energy bands.

III. RESULTS

In this section, we first examine the difference between the simple parabolic band dispersion and the non-parabolic solid-state band dispersion in the context of the semi-classical trajectory analysis. For this purpose, we employ the Kane band model [38]. Then, we elucidate the role of Umklapp scattering in the HHG by comparing the semi-classical trajectory model with the one-dimensional quantum electron dynamics simulation. Finally, we further explore the effect of more general scattering with the mean-free path approximation.

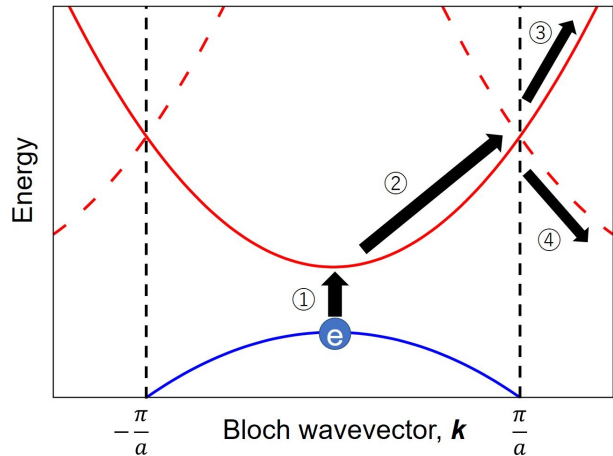


FIG. 1. Schematic picture of semi-classical trajectory dynamics and Umklapp scattering. The blue-solid line describes a valence band while the red-solid line describes an unfolded conduction band. The replicated unfolded-bands with the reciprocal lattice vector are indicated as the red-dashed lines.

A. Solid-state trajectory model without scattering

To study the solid-state HHG with the semi-classical model, we first examine the semi-classical trajectory analysis with the Kane band model [38] without the scattering contribution. The Kane band model is widely used to model the solid-state electronic band structures. For example, the seminal work for field-induced ionization by Keldysh [39], which finds applications in many fields [40–42], is based on the Kane band.

Here, we briefly assess the difference between the parabolic band dispersion and the solid-state Kane band dispersion in the semi-classical trajectory model of HHG. The parabolic energy dispersion is described as

$$\epsilon_{parabolic}(\mathbf{k}) = \epsilon_g + \frac{|\mathbf{k}|^2}{2\mu}, \quad (4)$$

where ϵ_g is the band gap, and μ is the electron-hole reduced mass. With the same parameters, the Kane band can be described as

$$\epsilon_{Kane}(\mathbf{k}) = \epsilon_g \sqrt{1 + \frac{|\mathbf{k}|^2}{\mu\epsilon_g}}. \quad (5)$$

According to previous works [34, 35] based on the semi-classical trajectory model, one can evaluate the cutoff energy of HHG as the maximum recombination energy among all possible trajectories under monochromatic laser fields. Figure 2 shows the cutoff energy U_c of the semi-classical trajectory model as a function of the square root of the ponderomotive energy $\sqrt{U_p}$, which is defined as $U_p = F_0^2/4\mu\omega_0^2$ with the laser field strength F_0 , the effective mass μ and the laser angular frequency ω_0 . The red-solid line shows the result of the Kane band

model, while the green-dashed line shows that of the parabolic band model. For the parabolic dispersion case, the cutoff energy U_c is described by the well-known formula as [34]

$$U_c^{(parabolic)} = \epsilon_g + 3.17U_p. \quad (6)$$

As seen from Fig. 2, in the weak field region (small U_p region), the two models give the similar cutoff energy. This observation can be understood by a fact that the Kane band model is reduced to the parabolic band model in the small wavenumber limit as $\epsilon_{Kane}(\mathbf{k}) \rightarrow \epsilon_g + |\mathbf{k}|^2/2\mu$, ($|\mathbf{k}| \rightarrow 0$). As seen from Fig. 2, the two models show qualitatively different behaviors in the strong field region: the cutoff energy of the Kane band model is proportional to the field strength, $F_0 \sim \sqrt{U_p}$, while that of the parabolic band model is proportional to the square of the field strength. The quadratic field-strength dependence of the parabolic band model is consistent with the cutoff energy of the gas-phase HHG while the linear field-strength dependence is consistent with the reported feature of the solid-state HHG [22–24].

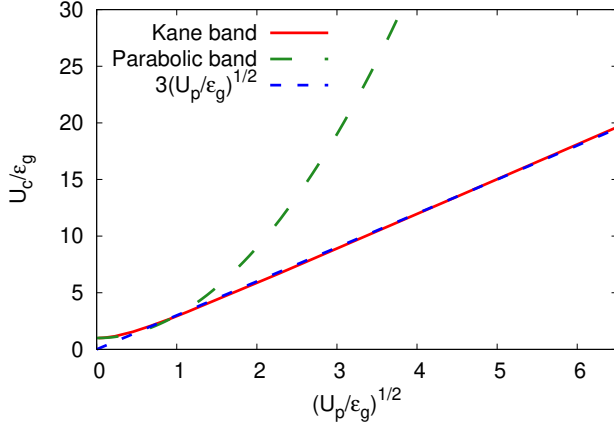


FIG. 2. Cutoff energy of the HHG U_c as a function of applied laser field strength F_0 , which is proportional to the square root of the ponderomotive energy U_p . The red-solid line shows the result of the Kane band model while the green-dashed line shows that of the parabolic band model. The blue-dotted line indicates the analytic line, $U_c/\epsilon_g = 3(U_p/\epsilon_g)^{1/2}$.

In Fig. 2, the blue-dotted line shows the analytic line, $U_c/\epsilon_g = 3(U_p/\epsilon_g)^{1/2}$. One sees that the analytic blue-dotted line shows nice agreement with the result of the Kane band model (red-solid line). Therefore, in the strong field limit, the cutoff energy of the Kane band model is well approximated as

$$U_c^{Kane} \approx 3\epsilon_g \sqrt{U_p/\epsilon_g} = \frac{3}{2}v_g^\infty \frac{F_0}{\omega_0}, \quad (7)$$

where v_g^∞ is the group electron-hole velocity of the Kane band model in the large $|\mathbf{k}|$ limit,

$$v_g^\infty = \lim_{|\mathbf{k}| \rightarrow \infty} \left| \frac{\partial}{\partial \mathbf{k}} \epsilon_{Kane}(\mathbf{k}) \right| = \sqrt{\frac{\epsilon_g}{\mu}}. \quad (8)$$

In contrast, the k -space semi-classical trajectory model [37] provides the following cutoff formula in the strong field limit

$$U_c^{k\text{-space}} = \epsilon_{Kane} \left(\frac{2F_0}{\omega_0} \right) \approx 2\sqrt{\frac{\epsilon_g}{\mu}} \frac{F_0}{\omega_0} = 2v_g^\infty \frac{F_0}{\omega_0}. \quad (9)$$

Note that the same cutoff expression has been derived for the analysis on graphene [43] with a similar consideration to the k -space trajectory. Comparing Eq. (7) and Eq. (9), the real-space trajectory model provides the smaller cutoff energy than the k -space trajectory model by a factor of 3/4. In the k -space trajectory model, the recombination is allowed at any instance of time. On the other hand, in the real-space trajectory model, the recombination is allowed only when paired electron and hole come to the same position. Therefore, the recombination events in the real-space trajectory model is a subset of those in the k -space model. Hence the cutoff energy of the real-space model is smaller than that of the k -space model by construction.

B. Umklapp scattering contribution to the HHG

Here, we investigate the role of Umklapp scattering in the semi-classical trajectory model. For this purpose, we compare the semi-classical trajectory model with the one-dimensional quantum mechanical (1D-QM) simulation. We employ the same model for the 1D-QM simulation as the previous work [37]. We first briefly explain the 1D-QM simulation, and then introduce the corresponding semi-classical trajectory model with Umklapp scattering.

The 1D-QM system is described by the following single-particle Schrödinger equation

$$i\frac{\partial u_{b,k}(x,t)}{\partial t} = \left[\frac{1}{2} \left\{ -i\frac{\partial}{\partial x} + k + A(t) \right\}^2 + v(x) \right] u_{b,k}(x,t), \quad (10)$$

where $u_{b,k}(x,t)$ are periodic part of the Bloch orbitals with the band index b and the Bloch wavenumber k . Here, $A(t)$ is the spatially-uniform time-dependent vector potential and $v(x)$ is the single-particle potential. For the single-particle potential $v(x)$, we employ the Mathieu-type lattice potential

$$V(x) = V_0 \cos \left(\frac{2\pi}{L} x \right), \quad (11)$$

where the potential height V_0 is set to 0.37 a.u. and the lattice constant L is set to 8 a.u.

In this work, the system is discretized by grid points for both real and crystal momentum spaces. The real-space unit-cell is discretized with 30 equally spaced grid points, and the first Brillouin zone is discretized with 352 uniformly spaced grid points. For the time propagation of the time-dependent Schrödinger equation we employ

the Taylor expansion scheme [44] with the single time step Δt set to 1 attosecond.

Figure 3 (a) shows the computed band structure of the 1D-QM model. The bottom two bands are treated as valence bands, and all the other bands are treated as the conduction bands. For the comparison with the semi-classical trajectory model, we fit the band structure of the 1D-QM model by the Kane band model. Figure 3 (b) shows the Kane band $\epsilon_{Kane}(k)$ and the particle-hole energy band structure of the 1D-QM model. The particle-hole energy bands are defined by the difference between the conduction bands and the top valence band as $\epsilon_{c,k} - \epsilon_{v,k}$, and they are unfolded in Fig. 3 (b). Here, the effective mass μ of the Kane band model is set to $0.083m_e$, and the band gap ϵ_g is set to 4.18 eV. These values are extracted from the 1D-QM model.

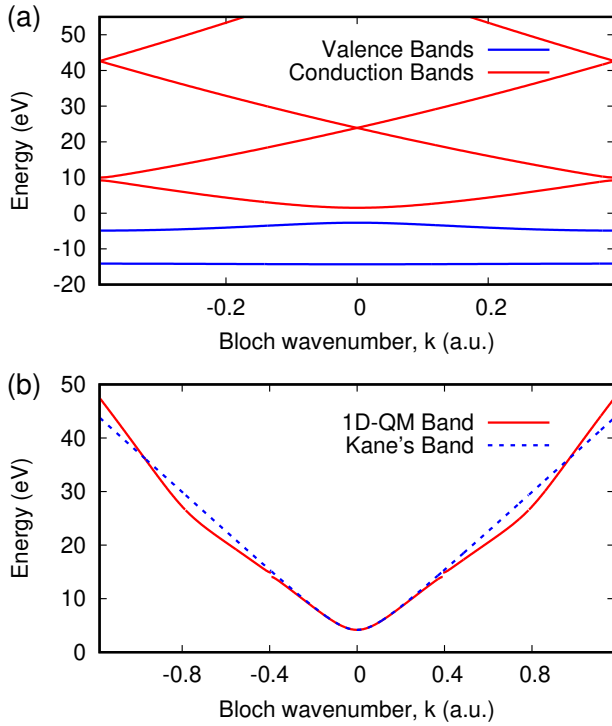


FIG. 3. (a) Electronic band structure of the one-dimensional quantum systems described by the Matthieu-type lattice potential, Eq. (11). The valence bands are shown as the blue lines while the conduction bands are shown as the red lines. (b) Comparison of the Kane band (blue-dotted) and the electron-hole band (red-solid), which is defined as the energy difference between the conduction bands and the top valence band, $\epsilon_{c,k} - \epsilon_{v,k}$.

We evaluate the HHG spectrum of the 1D-QM model by exactly solving numerically the time-dependent Schrödinger equation, Eq. (10), using the following form for the applied vector potential:

$$A(t) = \frac{F_0}{\omega_0} \sin^4\left(\frac{\pi}{\tau}t\right) \sin(\omega_0 t) \quad (12)$$

in the duration $0 < t < \tau$ and zero outside. Here, τ is

the full duration of the pulse. In this work, we set the mean photon energy $\hbar\omega_0$ to 387 meV (with corresponding wavelength 3200 nm), and the full duration of the pulse τ to 96.1 fs (equivalent to 9 periods of the mean photon frequency) according to the previous work [37].

During the time propagation, the electric current $J(t)$ can be evaluated by

$$J(t) = -\sum_{b=1}^2 \frac{1}{2\pi} \int_{-\pi/L}^{\pi/L} dk \times \int_0^L dx u_{bk}^*(x, t) \left[-i \frac{\partial}{\partial x} + k + A(t) \right] u_{b,k}(x, t). \quad (13)$$

Furthermore, the HHG spectrum $I(\omega)$ can be evaluated as the Fourier transform of the current as

$$I(\omega) \sim \omega^2 \left| \int_0^{T_{pulse}} dt \sin^4\left(\frac{\pi}{\tau}t\right) J(t) e^{i\omega t} \right|^2, \quad (14)$$

where the Fourier transform of the current is evaluated with the same envelope function as the applied laser pulse.

Figure 4 shows the computed power spectrum of the HHG from 1D-QM model with the field strength of $F_0 = 0.165$ V/Å, showing the clear multiple plateaus. The multi-plateau feature was investigated with the k -space semi-classical trajectory model, and it was explained by the ladder climbing process in the band structure [37]. In this subsection, we explore the multi-plateau feature based on the real-space semi-classical trajectory with the scattering effect.

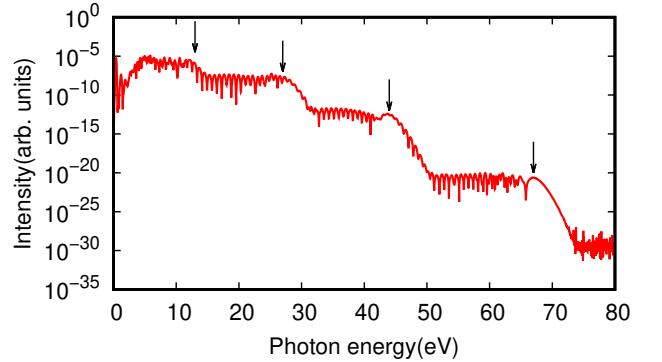


FIG. 4. HHG spectrum computed by the quantum simulation with the field strength of $F_0 = 0.165$ V/Å. The cut-off energy of multiple plateaus are indicated by black arrows around 13, 28, 44, and 68 eV.

In our model we explore the multi-plateau feature based on both the k -space and the real-space semi-classical trajectory with the scattering effect. Figure 5 shows the HHG spectra as functions of the applied field strength F_0 . One can see the formation of the multi-plateau feature with increase of the field strength. To

assess the semi-classical trajectory model, the computed cutoff energy with the Kane band model is also shown as the black-solid line (non-scattered), which is nothing but the red-solid line shown in Fig. 2. One sees that the first cutoff of the 1D-QM model is captured by the semi-classical trajectory model without scattering (black line).

To study the role of scattering, we evaluate the maximum recombination energy among all possible scattered trajectories as the cutoff energy of the scattered trajectory. In Fig. 5, the red line shows the maximum recombination energy among the single-scattered trajectories, and the orange line shows that among the double-scattered trajectories. By comparing the cutoff energies of the scattered trajectories with the HHG spectra of the 1D-QM model, one sees that the single-scattering trajectories (red line) provide the second cutoff of the 1D-QM simulation while the double-scattering trajectories provide the third cutoff. Therefore, the formation of the multi-plateau feature in the HHG spectrum can be understood as the consequence of Umklapp scattering. This real-space scattering interpretation is a complementary picture of the previous ladder climbing picture in the k -space [37].

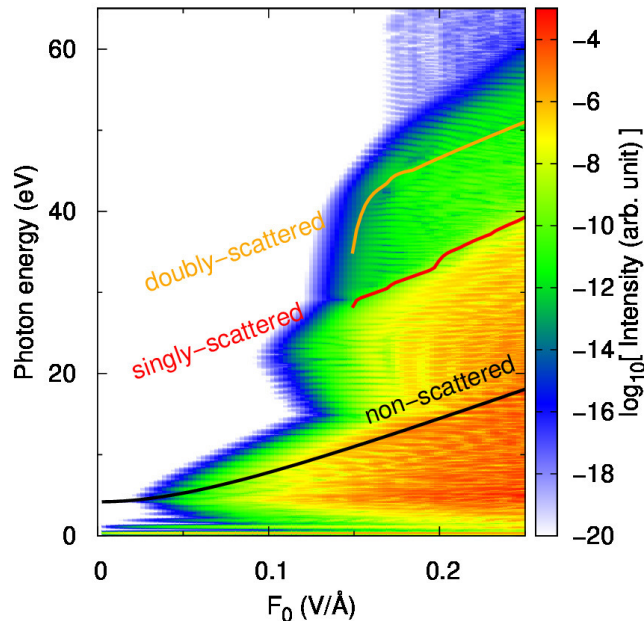


FIG. 5. Spectra of HHG computed by the 1D-QM simulation as functions of the field strength, F_0 . The cutoff energies computed with the semi-classical trajectory model are also shown: The black line shows the result without scattering, the red line shows that of singly-scattered trajectories, and the orange line shows that of doubly-scattered trajectories.

To study further details of the scattering effect in the HHG from solids, we elucidate the temporal structure of HHG. For this purpose, we perform the Gabor transformation to the current $J(t)$ with the time window function

whose the full width of the half maximum (FWHM) is 1.78 fs. The computed temporal evolution of HHG from the 1D-QM model is shown in Fig. 6. Here, the field strength F_0 is set to 0.165 V/Å. Note that, in all the panels of Fig. 6, the same result of the 1D-QM model is shown. In addition to the 1D-QM result, the recombination energy and timing evaluated by the semi-classical trajectory model of different number of scattering are depicted in different panels; The panel (a), (b), and (c) show the results of non-scattered, singly-scattered, and doubly-scattered trajectories, respectively.

As seen from Fig. 6 (a), the non-scattered trajectories contribute only to the first plateau of HHG. In contrast, in Fig. 6 (b), the single-scattered trajectories show the contribution to the second plateau (around 13 to 28 eV). Furthermore, from Fig. 6 (c), the double-scattered trajectories contribute to the formation of the third plateau (around 28 to 44 eV). Therefore, Umklapp scattering processes open higher energy channels for the trajectory dynamics, resulting in the multi-plateau feature as a consequence of the multiple scatterings.

In Fig. 6 (a) to (c), one sees that the real-space trajectory model fairly captures the recombination energy and timings. This is a distinct feature from the k -space trajectory model where the recombination timing is arbitrary and can occur any instance of time. This fact indicates the importance of the real-space trajectory picture to describe the HHG even with scattering process.

Note that the present real-space trajectory model does not capture all the features of the 1D-QM simulation. For example, in Fig. 6 (c) semi-classical model fails to reproduce the signals on the left side of the classical prediction in the second plateau or the signal on the right side of the classical prediction in the third plateau. These additional features can be understood by the quantum wavepacket effect. In the present semi-classical model, the excitation occurs only at the optical gap, and the scattering takes place only at the band crossing points. However, in the quantum system, the excitation and scattering can occur with finite width in the k -space. As a result, the full quantum systems can involve more trajectories and add the additional features to the semi-classical model.

C. Loss of trajectories by electron scattering in the HHG

In the above analysis, we investigated the role of Umklapp scattering in one-dimensional systems. Because only the forward or backward scatterings are allowed in the one-dimensional systems, the scattered trajectory can be recombined with relatively high probability. In contrast, the contribution from scattered trajectories in two- and three-dimensional systems is expected to be significantly suppressed since trajectories can be scattered into a variety of directions, thus reducing the probability of recombination for returning trajectories. In addition to the consideration on dimensionality, there are many scatter-

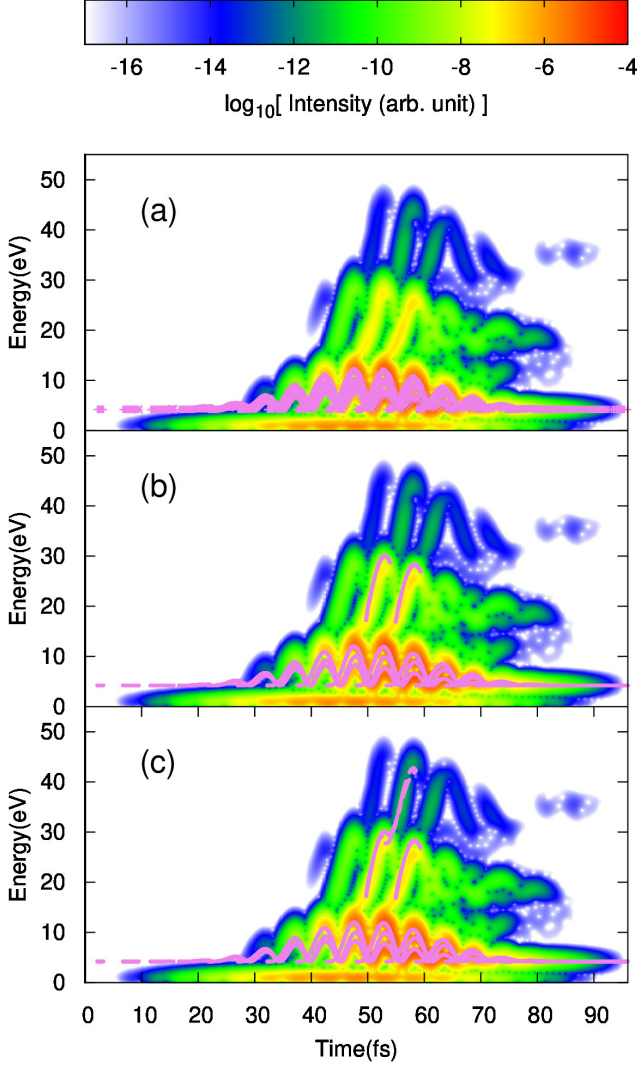


FIG. 6. Temporal evolution of the HHG computed with the 1D-QM simulation. The purple dots describe the emitted photon energy and the emission timing, computed by the semi-classical trajectory model. Each panel shows the contribution from semi-classical trajectories with different number of scattering: (a) No scattering, (b) single scattering, and (c) double scattering.

ing processes in solids other than Umklapp scattering. These scattering processes may also play an important role in solid-phase HHG.

In order to assess the impact of the suppression of HHG by various scattering processes in the higher-dimensional space, we consider a simple mean-free-path model instead of the trajectory branching mentioned above. In the mean-free-path model, we compute the trajectory length $l_d(t)$ as

$$l_d(t) = \int_{t_0}^t dt' |\mathbf{v}(\mathbf{K}(t'))|. \quad (15)$$

Furthermore, we simply assume that semi-classical tra-

jectories do not contribute to HHG anymore once the trajectory length reaches a given mean-free-path length, l_{MFP} . Integrating this destructive contribution of scattering into the semi-classical trajectory model instead of the trajectory-branching process, we evaluate the maximum recombination energy among all trajectories before their trajectory length reaches the mean-free-path length.

Figure 7 shows the computed cutoff energy from the semi-classical trajectory model for different mean-free-path length l_{MFP} as functions of the applied laser wavelength under the fixed field strength $F_0 = 0.165$ V/Å. As seen from Fig. 7, the trajectory model without scattering (black) shows almost linear dependency in the long wavelength region. This behavior can be understood as the asymptotic linear dispersion of the Kane band model in the large Bloch wavevector region, as described in Eq. (7).

Once the loss of trajectories is introduced via the mean-free-path approximation, the semi-classical trajectory model shows the saturation of the HHG cutoff energy in the long wavelength region. This saturation can be understood by a fact that, even if laser fields with longer wavelength can induce higher energy trajectories, such higher-energy trajectories have longer travel distance and they are lost by the scattering process.

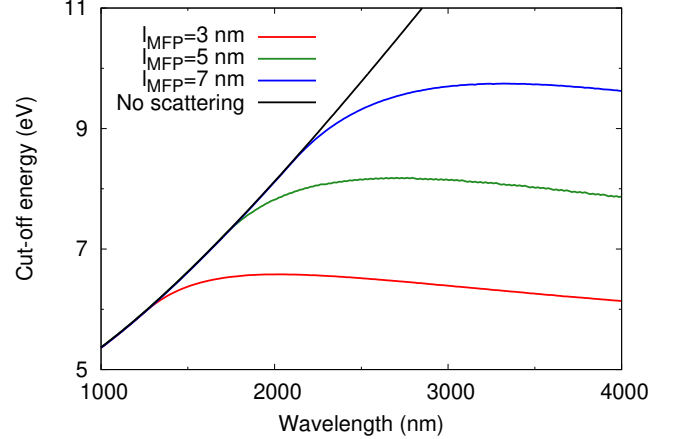


FIG. 7. Wavelength dependence of the cutoff energy of HHG, evaluated by the semi-classical trajectory model with the mean-free-path approximation. The results with several mean-free-path length l_{MFP} are described. The result without scattering process is also shown as the black line.

One sees that the cutoff energy of the trajectory model with the scattering effect in Fig. 7 becomes almost constant in the long wavelength region. This behavior is nothing but the wavelength independence of the HHG cutoff energy, and it is consistent with one of the features of the HHG from solids [22, 24, 25]. Thus, the loss of trajectories by scattering can be one of the physical mechanisms of the wavelength independence of the cutoff energy of HHG from solids. In order to clarify the details of the trajectory loss effect, the comparison of the trajectory model with the three-dimensional re-

alistic simulations such as the *ab-initio* time-dependent density functional theory simulation, which also captures the wavelength independence of the HHG cutoff energy [25], will be useful. However, such analysis is beyond the scope of the present work, and will be investigated in the future.

IV. SUMMARY

We studied the effect of electron scattering in the HHG from solids based on the semi-classical trajectory description. We first extended the solid-state semi-classical trajectory model [35] by integrating the Umklapp scattering with the Kane band model [38]. The extended model has been examined by comparing with the one-dimensional quantum dynamical simulation used in Ref. [37]. As a result, the multi-plateau feature of the HHG spectra of the one-dimensional quantum model has been fairly captured by the contribution from the multiple Umklapp-scattered trajectories under the laser field acceleration. Therefore, we concluded that the multi-plateau feature is the consequence of the Umklapp scattering. In the previous work based on the k -space trajectory model [37], the same multi-plateau feature has been interpreted as the consequence of the ladder-climbing process in the electronic band structure. The two interpretations based on the real-space and k -space trajectories are equivalent but offers different views into the same phenomenon: the ladder-climbing process in k -space can be seen as the dynamics with Umklapp scattering in real-space.

We further examine the effect of Umklapp scattering by evaluating the recombination timing of electron-hole pairs and the emitted photon energy. By comparing the results of the semi-classical trajectory model with the temporal structure of the HHG spectra of the one-dimensional quantum model, we confirm that the semi-classical trajectory model with Umklapp scattering properly captures the timing and energy of the HHG from

solids. This fact demonstrates that the semi-classical real-space trajectories play an important role in the microscopic mechanism of the HHG from solids because the recombination timing is not determined in the purely k -space trajectory model, where the recombination can occur at any time instance.

Then, we explored other consequence of the electron scattering, considering that scattered trajectories in a higher-dimensional space are less likely to recombine. To take into account this effect, we evaluate the travel distance of each trajectory and disregard trajectories if their travel distance reaches a given mean-free-path length. We evaluated the wavelength dependence of the HHG cutoff energy by the semi-classical trajectory model with the mean-free-path approximation. As a result, we found that the cutoff energy is significantly suppressed under the longer wavelength laser driving since the longer wavelength laser field tends to induce longer travel distance for trajectories. In addition, we found that the cutoff energy is almost independent of the laser wavelength once the wavelength becomes long enough. This wavelength independence is consistent with a feature of the reported HHG from solids [22, 24, 25].

The above findings indicate that the real-space trajectory combined with scattering processes plays an essential role in the HHG from solids. Thus, the optical control of the real-space trajectories under scattering processes may further open a way to enhance and control the HHG from solids.

ACKNOWLEDGMENTS

This work was supported by the European Research Council (ERC-2015-AdG694097), the Cluster of Excellence 'Advanced Imaging of Matter' (AIM), and JST-CREST under Grant No. JP-MJCR16N5. S.A.S. gratefully acknowledges the fellowship from the Alexander von Humboldt Foundation.

-
- [1] G. Mourou, N. Fisch, V. Malkin, Z. Toroker, E. Khazanov, A. Sergeev, T. Tajima, and B. L. Garrec, *Optics Communications* **285**, 720 (2012).
 - [2] F. Krausz and M. I. Stockman, *Nature Photonics* **8**, 205 (2014).
 - [3] D. N. Basov, R. D. Averitt, and D. Hsieh, *Nature Materials* **16**, 1077 (2017).
 - [4] J. Flick, M. Ruggenthaler, H. Appel, and A. Rubio, *Proceedings of the National Academy of Sciences* **114**, 3026 (2017).
 - [5] P. N. Butcher and D. Cotter, *The elements of nonlinear optics*, Vol. 9 (Cambridge university press, 1990).
 - [6] R. W. Boyd, *Nonlinear Optics* (Academic Press, New York, 2008).
 - [7] M. Hentschel, R. Kienberger, C. Spielmann, G. A. Reider, N. Milosevic, T. Brabec, P. Corkum, U. Heinzmann, M. Drescher, and F. Krausz, *Nature* **414**, 509 (2001).
 - [8] T. Pfeifer, C. Spielmann, and G. Gerber, *Reports on Progress in Physics* **69**, 443 (2006).
 - [9] F. Krausz and M. Ivanov, *Rev. Mod. Phys.* **81**, 163 (2009).
 - [10] P. A. Franken, A. E. Hill, C. W. Peters, and G. Weinreich, *Phys. Rev. Lett.* **7**, 118 (1961).
 - [11] J. L. Krause, K. J. Schafer, and K. C. Kulander, *Phys. Rev. Lett.* **68**, 3535 (1992).
 - [12] K. J. Schafer, B. Yang, L. F. DiMauro, and K. C. Kulander, *Phys. Rev. Lett.* **70**, 1599 (1993).
 - [13] M. Lewenstein, P. Balcou, M. Y. Ivanov, A. LHuillier, and P. B. Corkum, *Physical Review A* **49**, 2117 (1994).
 - [14] A. McPherson, G. Gibson, H. Jara, U. Johann, T. S. Luk, I. A. McIntyre, K. Boyer, and C. K. Rhodes, *J. Opt. Soc.*

- Am. B **4**, 595 (1987).
- [15] M. Ferray, A. L'Huillier, X. F. Li, L. A. Lompre, G. Mainfray, and C. Manus, *Journal of Physics B: Atomic, Molecular and Optical Physics* **21**, L31 (1988).
 - [16] J. Itatani, J. Levesque, D. Zeidler, H. Niikura, H. Pépin, J. C. Kieffer, P. B. Corkum, and D. M. Villeneuve, *Nature* **432**, 867 (2004).
 - [17] E. Goulielmakis, Z.-H. Loh, A. Wirth, R. Santra, N. Rohringer, V. S. Yakovlev, S. Zherebtsov, T. Pfeifer, A. M. Azzeer, M. F. Kling, S. R. Leone, and F. Krausz, *Nature* **466**, 739 (2010).
 - [18] M. Schultze, K. Ramasesha, C. D. Pemmaraju, S. A. Sato, D. Whitmore, A. Gandman, J. S. Prell, L. J. Borja, D. Prendergast, K. Yabana, D. M. Neumark, and S. R. Leone, *Science* **346**, 1348 (2014).
 - [19] M. Lucchini, S. A. Sato, A. Ludwig, J. Herrmann, M. Volkov, L. Kasmi, Y. Shinohara, K. Yabana, L. Gallmann, and U. Keller, *Science* **353**, 916 (2016).
 - [20] M. Volkov, S. A. Sato, F. Schlaepfer, L. Kasmi, N. Hartmann, M. Lucchini, L. Gallmann, A. Rubio, and U. Keller, *Nature Physics* **15**, 1145 (2019).
 - [21] F. Siegrist, J. A. Gessner, M. Ossiander, C. Denker, Y.-P. Chang, M. C. Schröder, A. Guggenmos, Y. Cui, J. Walowski, U. Martens, J. K. Dewhurst, U. Kleineberg, M. Münzenberg, S. Sharma, and M. Schultze, *Nature* **571**, 240 (2019).
 - [22] S. Ghimire, A. D. DiChiara, E. Sistrunk, P. Agostini, L. F. DiMauro, and D. A. Reis, *Nature Physics* **7**, 138 (2011).
 - [23] O. Schubert, M. Hohenleutner, F. Langer, B. Urbanek, C. Lange, U. Huttner, D. Golde, T. Meier, M. Kira, S. W. Koch, and R. Huber, *Nature Photonics* **8**, 119 (2014).
 - [24] T. T. Luu, M. Garg, S. Y. Kruchinin, A. Moulet, M. T. Hassan, and E. Goulielmakis, *Nature* **521**, 498 (2015).
 - [25] N. Tancogne-Dejean, O. D. Mücke, F. X. Kärtner, and A. Rubio, *Phys. Rev. Lett.* **118**, 087403 (2017).
 - [26] N. Yoshikawa, T. Tamaya, and K. Tanaka, *Science* **356**, 736 (2017).
 - [27] N. Tancogne-Dejean, O. D. Mücke, F. X. Kärtner, and A. Rubio, *Nature Communications* **8**, 745 (2017).
 - [28] H. Liu, Y. Li, Y. S. You, S. Ghimire, T. F. Heinz, and D. A. Reis, *Nature Physics* **13**, 262 (2017).
 - [29] N. Tancogne-Dejean and A. Rubio, *Science Advances* **4**, eaao5207 (2018).
 - [30] G. Le Breton, A. Rubio, and N. Tancogne-Dejean, *Phys. Rev. B* **98**, 165308 (2018).
 - [31] S. Ghimire and D. A. Reis, *Nature Physics* **15**, 10 (2019).
 - [32] K. Kulander, K. Schafer, and J. Krause, in *Super-Intense Laser-Atom Physics* (Springer, 1993) pp. 95–110.
 - [33] P. B. Corkum, *Phys. Rev. Lett.* **71**, 1994 (1993).
 - [34] M. Lewenstein, P. Balcou, M. Y. Ivanov, A. L'Huillier, and P. B. Corkum, *Phys. Rev. A* **49**, 2117 (1994).
 - [35] G. Vampa, C. R. McDonald, G. Orlando, P. B. Corkum, and T. Brabec, *Phys. Rev. B* **91**, 064302 (2015).
 - [36] G. Ndabashimiye, S. Ghimire, M. Wu, D. A. Browne, K. J. Schafer, M. B. Gaarde, and D. A. Reis, *Nature* **534**, 520 (2016).
 - [37] T. Ikemachi, Y. Shinohara, T. Sato, J. Yumoto, M. Kuwata-Gonokami, and K. L. Ishikawa, *Phys. Rev. A* **95**, 043416 (2017).
 - [38] E. O. Kane, *Journal of Physics and Chemistry of Solids* **1**, 249 (1957).
 - [39] L. Keldysh, *Sov. Phys. JETP* **20**, 1307 (1965).
 - [40] P. Balling and J. Schou, *Rep. Prog. Phys.* **76**, 036502 (2013).
 - [41] A.-C. Tien, S. Backus, H. Kapteyn, M. Murnane, and G. Mourou, *Phys. Rev. Lett.* **82**, 3883 (1999).
 - [42] P. Jürgens, M. Jupé, M. Gyamfi, and D. Ristau, *Proc.SPIE* **10014**, 100141C (2016).
 - [43] L. A. Chizhova, F. Libisch, and J. Burgdörfer, *Phys. Rev. B* **95**, 085436 (2017).
 - [44] K. Yabana and G. F. Bertsch, *Phys. Rev. B* **54**, 4484 (1996).